How the Geometry and Mechanics of Bighorn Sheep Horns Mitigate the Effects of Impact and Reduce the Head Injury Criterion

Benjamin B. Wheatley[1*], Emma C. Gilmore[2], Luca H. Fuller[2], Aaron M. Drake[3], Seth W. Donahue[2]

[1]Department of Mechanical Engineering, Bucknell University, Lewisburg PA

[2]Department of Biomedical Engineering, University of Massachusetts Amherst, Amherst MA

[3]Function First Innovative Design, LLC, Denver, CO

*Corresponding author:

Benjamin B Wheatley

Department of Mechanical Engineering

Academic East 302

Bucknell University

Lewisburg, PA 17837-2005

(570) 577-3883

b.wheatley@bucknell.edu

Keywords: ovis canadensis, impact biomechanics, finite element analysis, bioinspired design, chronic traumatic encephalopathy

Abstract

Male bighorn sheep (*Ovis canadensis*) participate in seasonal ramming bouts that can last for hours, yet they do not appear to suffer significant brain injury. Previous work has shown that the keratin-rich horn and boney horncore may play an important role in mitigating brain injury by reducing brain cavity accelerations through energy dissipating elastic mechanisms. However, the extent to which specific horn shapes (such as the tapered spiral of bighorn sheep) may reduce accelerations post-impact remains unclear. Thus, the goals of this work were to 1) quantify bighorn sheep horn shape, particularly the cross-sectional areal properties related to bending that largely dictate post-impact deformations, and 2) investigate the effects of different tapered horn shapes on reducing post-impact accelerations in an impact model with finite element analysis. Cross-sectional areal properties indicate bighorn sheep horns have a medial-lateral bending preference at the horn tip ($p=0.006$), which is likely to dissipate energy through medial-lateral horn tip oscillations after impact. Finite element modeling showed bighorn sheep native horn geometry reduced the head injury criterion (HIC_{15}) by 48% compared to horns with cross-sections rotated by 90 degrees to have a cranial-caudal bending preference, and by 125% compared to a circular tapered spiral model. These results suggest that the tapered spiral horn shape of bighorn sheep is advantageous for dissipating energy through elastic mechanisms following an impact. These findings can be used to broadly inform the design of improved safety equipment and impact systems.

1. Introduction

Mild traumatic brain injuries (i.e. concussions) are a major health concern due to their prevalence and permanent impact on brain function. Soldiers and athletes are at particularly high risk for concussions due to increased exposure to head trauma via impact or explosive blasts. The annual incidence rate of traumatic brain injury in active-duty Army service members was 2.7% in 2011("Report to Congress on Traumatic Brain Injury in the United States," 2019). In 2017, 15.1% of United States high school students reported having experienced at least one concussion due to athletics (DePadilla, 2018). While the etiology of these injuries is not fully understood, translational and rotational accelerations of the brain cavity have been correlated with concussion occurrence (Meaney and Smith, 2011). The head injury criterion (HIC) is a standardized measurement that identifies the likelihood of a head injury resulting from an acceleration profile (Hutchinson et al., 1998). Recent studies have shown links between mild traumatic brain injuries and chronic traumatic encephalopathy, a condition of long-term neurodegeneration (Daneshvar et al., 2015; Finkbeiner et al., 2016). Together, these findings have led to increased investment in the development of novel head protection systems capable of preventing concussive injury.

To expedite the development of brain injury mitigation technology, it is worthwhile to study animal species that have evolved to withstand routine, repetitive head impacts via pecking or head-butting. Woodpeckers, male sperm whales, pachycephalosaurian dinosaurs, and bighorn sheep rams are all believed to possess anatomical structures and physiological mechanisms optimized for head impact (Drake et al., 2016; Panagiotopoulou et al., 2016; Snively and Theodor, 2011; Wang et al., 2011)**.** Recent studies on the tauopathies of woodpeckers and headbutting bovids have found some evidence of traumatic brain injury in these animals (Ackermans et al., 2022; Farah et al., 2018). However, in muskoxen and bighorn sheep, signs of brain injury were more prevalent in female samples suggesting the thicker skulls and larger horns of males offer some level of injury mitigation (Ackermans et al., 2022). Furthermore, the lack of overt signs of brain injury (i.e. unconsciousness) provides additional motivation to study the protective role of these structures during ramming.

Male bighorn sheep weigh between 60-135 kg and participate in seasonal ramming bouts that can last for several hours (Geist, 1974; "Mountain Sheep of North America," 2017). Individual ramming events have been associated with velocities exceeding 5 m/s and impact forces as high as 3200 N (Kitchener, 1988). Computational modeling has demonstrated that horn and horncore structures are critical for dissipating impact energy and reducing brain cavity accelerations (Drake et al., 2016). In physiological models, peak translational and rotational accelerations of the brain cavity have been estimated to be approximately 400 g and 7400 rad/s^2, respectively (Drake et al., 2016). Comparatively, male high school football players weighing ~90 ± 13 kg experienced impacts at 11 m/s generating forces of ~1300 N, linear accelerations of ~25 g, and rotational accelerations of ~1600 rad/s^2 (Broglio et al., 2010, 2009). In this study, concussive injuries were associated with mean linear accelerations of ~105 g and mean rotational accelerations of 7230 rad/s^2. Injury threshold values within a similar range have also been

reported for collegiate (~103 g and 5300 rad/s^2) (Guskiewicz et al., 2007)and professional American football (98 g and ~6400 rad/s^2) (Pellman et al., 2003). It is interesting that bighorn sheep rams show minimal evidence of traumatic brain injury despite exceptionally high translational accelerations during ramming. It is possible that bighorn sheep brain tissue is less susceptible to mechanically induced damage than human brain tissue resulting in a higher injury threshold, though no data is currently available for this comparison. However, it was also demonstrated that removing various anatomical structures from the horn and horncore resulted in even higher accelerations during ramming (Drake et al., 2016). Understanding the specific mechanisms that result in reduction of brain cavity accelerations during ramming has clear implications for brain injury prevention of humans and may inspired novel helmet technology.

The physiological mechanisms dissipating impact energy during bighorn sheep ramming are believed to be the frontal sinus, tapered spiral horn shape, and porous bone within the horn (Aguirre et al., 2020; Drake et al., 2016; Maity and Tekalur, 2011). At the macroscale, bighorn sheep horns consist of a boney horncore sheathed by a keratin-rich horn. The horncore consists of a dense outer cortical bone shell with a porous core consisting of interconnected sail-like boney plates, known as velar bone (Fuller and Donahue, 2021). Much experimental work has been done to characterize the material properties and microstructure of bighorn sheep horn (Huang et al., 2019, 2017; Tombolato et al., 2010; Trim et al., 2011) and horncore bone (Fuller and Donahue, 2021). Computational models of bighorn sheep ramming have also been developed to study the mechanics of impact (Drake et al., 2016; Johnson et al., 2021; Maity and Tekalur, 2011). Specifically, our previous work demonstrated that removal of the distal half of the horn results in a ~50% increase in translational accelerations of the brain cavity and removal of the velar bone resulted in a >400% increase in rotational accelerations (Drake et al., 2016). However, less is known about how the unique horn shape may contribute to injury mitigation. It was previously suggested that horn tip oscillations intentionally directed into side-to-side (medial-lateral) motion may be one mechanism of energy dissipation. Additionally, geometry has been shown to affect dynamic wave propagation in other curved structures (Johnson et al., 2014). For example, the woodpecker's curved hyoid bone absorbs impact energy during pecking and has been used for bioinspired design of impact mitigation structures (Lee et al., 2016). It is possible that the unique tapered spiral shape of ram horns may be advantageous for energy dissipation and injury mitigation during ramming.

Bioinspiration and biomimetic efforts based upon animal horns, especially bighorn sheep horns, have largely focused on the keratin microstructure. These studies have investigated or leveraged the pore-like microstructure common in bighorn sheep keratin, the foam-like structure of the boney horncore, gradients in the porosity and moisture content of horn and hoof keratin, and the energy released during delamination of horn keratin layers (Ha and Lu, 2020; Islam et al., 2021; Naleway et al., 2015; Wang et al., 2016). In regards to macrostructure of animal horns, Zhou et al., 2021 showed that a bioinspired yak horn exhibited greater specific energy absorption than most other general shapes (Zhou et al., 2021). However, to the best of the authors'

knowledge, there has not yet been an effort to characterize how biomimetic tapered spirals, such as bighorn sheep horns, mitigate the effect of impact through directional oscillations.

The current study thus aimed to 1) quantify bighorn sheep horn shape across multiple individuals, and 2) determine the effect of various tapered spiral geometries in impact mitigation. We hypothesized that bighorn sheep horns collectively exhibit a transition from having no directional bending preference near the base of the horn to a medial-lateral bending preference at the horn tip to facilitate side-to-side oscillations. We also hypothesized that the specific horn spiral shape exhibits superior impact mitigating qualities in comparison to other spiral shapes. Results from this study may be used to guide future modeling efforts to study the contribution of various horn shape characteristics related to energy absorption and reduction of brain cavity accelerations during impact. Furthermore, a better understanding of these macrostructural features of bighorn sheep horns may provide useful information for the design of future impact structures, such as helmets.

2. Methods

2.1 Samples

Four male bighorn sheep skulls were provided for research purposes by the Colorado Department of Natural Resources under Colorado Parks and Wildlife scientific collection license number 14SALV2052A2. Animals were killed in motor vehicle accidents and frozen shortly after death. Rams included in this study were all adults estimated to be between 5 – 8 years old using the common technique of counting annual growth rings visible on the horns (Geist, 1966).

2.2 Bighorn Sheep Horn Pre-Processing

All four skulls were scanned using x-ray computed tomography, with specific scanning parameters as previously detailed (Drake et al., 2016). Sets of DICOM images for each individual were imported into Seg3D software for image segmentation (http://www.seg3d.org). Image slices were acquired in the transverse plane, which along with the frontal and sagittal planes describe the anatomical orientations of the bighorn sheep skull and horns (Figure 1). The images were subject to thresholding to separate bone and horn, manually cleaned, and an ISO surface was generated from each segment for exportation as ASCII STL files. After segmentation, the horn and bone geometries were separately imported into MeshLab and processed with a quadratic edge collapse decimation filter to reduce the mesh size and a Laplacian smoothing filter to reduce pixelation (Cignoni et al., 2008). Preliminary studies showed that reducing faces to 1% of the original number was sufficient to maintain accurate geometry at a reasonable computational cost and the optimal number of smoothing steps was found to be approximately eight steps for bone and six steps for horn. Horn and bone STL files were imported into SolidWorks (Dassault Systèmes) as surface bodies to be analyzed.

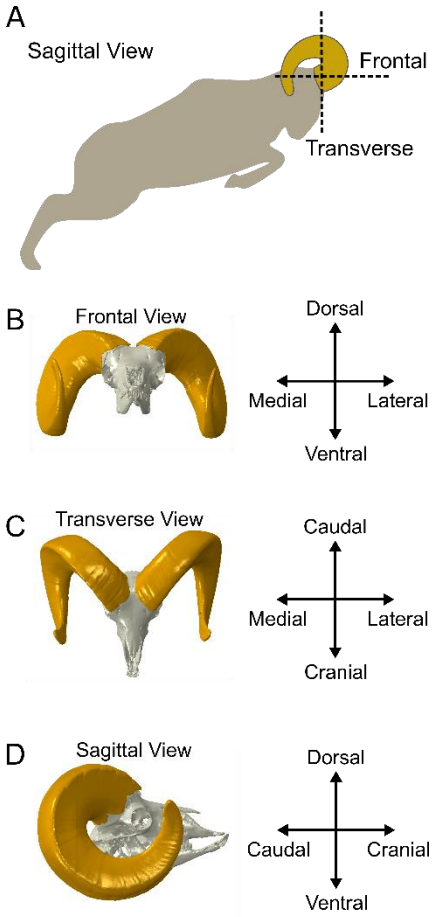

Figure 1. A) A bighorn sheep outlined in the sagittal plane during a ramming bout, showing the approximate impact direction. The frontal and transverse planes are indicated by dashed lines. B) Frontal plane view, with medial-lateral and dorsal-ventral axes. C) Transverse plane view, with medial-lateral and cranial-caudal axes. D) Sagittal plane view, with cranial-caudal and dorsal-ventral axes.

2.3 Shape Characterization

All horn and horncore shape characterization was completed in SolidWorks (Dassault Systèmes). The first step in shape characterization was determining the path of the centerline of each horn. This centerline provided a representation of each horn's helicoidal shape from which specific shape measurements and horn and horncore cross-sections could be determined. First, in the sagittal plane, a spline was drawn along the outer curvature of the horn and nine evenly spaced lines were sketched perpendicular to the spline with midpoints (Figure 2). Similarly, in the frontal plane, a spline was drawn along the outer curvature of the horn, again with nine evenly spaced perpendicular lines and midpoints (Figure 2). From the midpoint of each of the eighteen perpendicular lines (nine sagittal, nine frontal), axes were generated orthogonal to the corresponding plane. The intersections of each of the paired axes (sagittal and frontal) produced nine points in space, from which a centerline was created using a 3D spline (Figure 2). When necessary, a similar procedure was used in the transverse plane only for the distal portion of full

curl horns. This third view was required for larger horns because the distal portion of the horn overlapped itself in the frontal plane and could not be viewed properly (Figure 2). The overall centerline length and lateral centerline excursion (lateral distance from base to horn tip) were also computed.

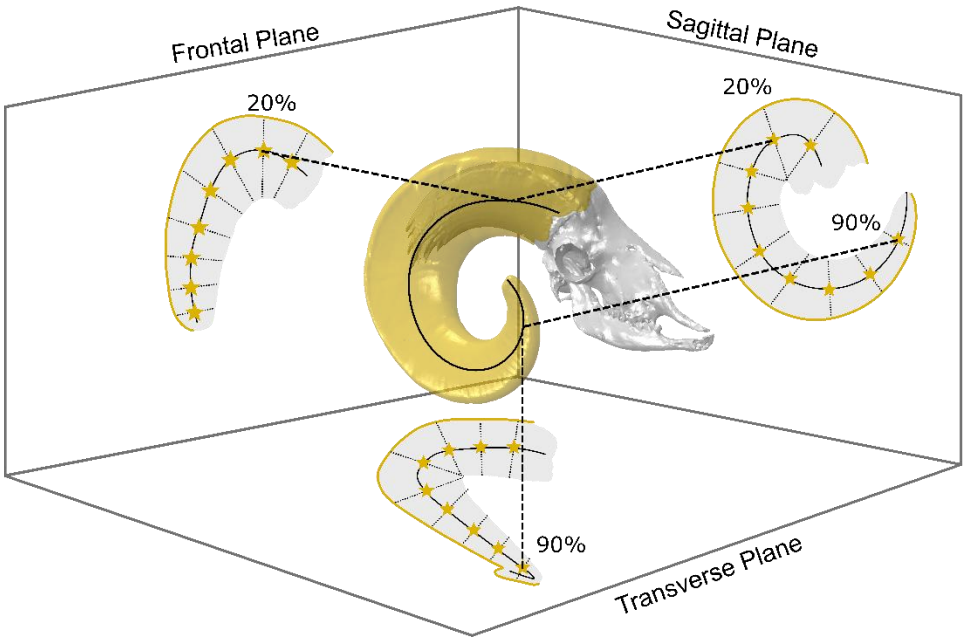

Figure 2. Procedure to determine horn centerline. The outline of each horn (yellow) was first traced in the sagittal and frontal planes, then perpendicular lines (dotted grey) were drawn at 10% intervals with midpoints (yellow stars). Orthogonal axes (dashed black) are drawn from each midpoint, normal to the corresponding plane (frontal or sagittal). Paired orthogonal axes (i.e. 20% sagittal and 20% frontal) intersect in 3D space, resulting in nine points that guide a 3D spline to create the centerline (solid black). For longer, full-curl horns, transverse and sagittal planes were used at the distal tip due to horn overlap in the frontal plane. Representative centerline points at 20% and 90% of total length are shown.

Horn cross-sections were defined with planes normal to the centerline and coincident with the same points used to define the centerline. The intersection curve tool was used to make cross-section sketches where these planes intersect the horn and horncore meshes. This resulted in nine cross-sections, evenly spaced at 10% intervals and labeled accordingly, from the proximal base (10% cross-section) to the distal tip (90% cross-section). The most proximal cross-sections (0% centerline length) were excluded because of imperfect geometry at the base. Additionally, cross-sections at the horn tip (100% centerline length) were singular points based on this methodology, and were also excluded from the analysis. Combined centers of mass for the bone and horn cross-sections were calculated using vector math and the parallel axis theorem. Next, a local coordinate system was defined at the combined center of mass of each cross-section with three axes corresponding to the anatomical planes. Local axes were defined by the intersection of the horn cross-section and reference planes parallel to the anatomical planes and coincident to the

combined center of mass (Figure 3). As a result, local sagittal, transverse, and frontal axes were defined for each cross-section.

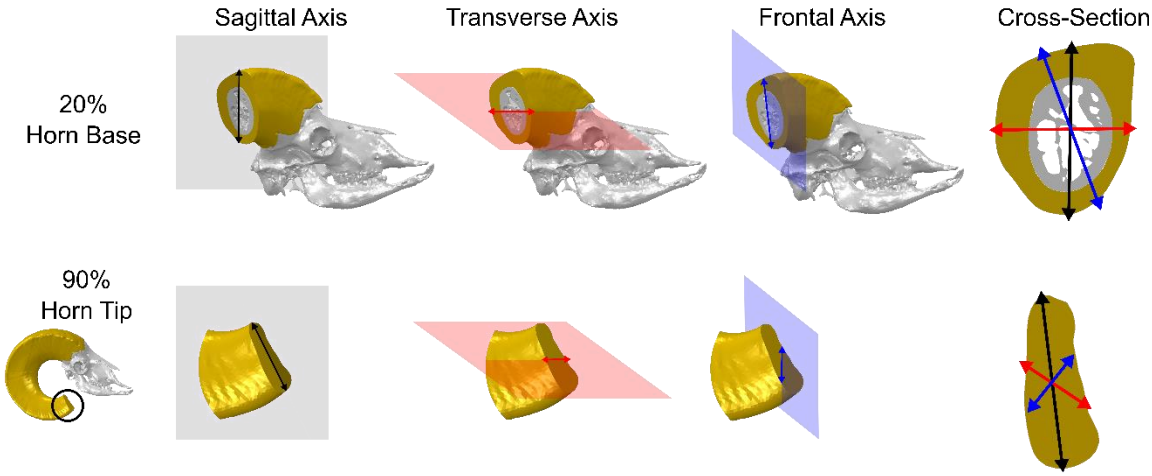

Figure 3. Definition of the local axes for each cross section. The top row shows a cross-section at 20% (horn base) with the sagittal plane and axis (black), the transverse plane and axis (red), and the frontal plane and axis (blue). All three axes are shown on the cross-section in the top right. The bottom row is similar for a 90% (horn tip) cross-section.

Second moments of area (I) and flexural rigidities (D) of each cross-section were calculated about the local axes with the parallel axis theorem to determine the bending resistance throughout the horn length (Equation 1). The second moments of area (I_S, I_F, and I_T), flexural rigidities (D_s, D_F, and D_T), and product moments of area were computed about the combined center of mass by SolidWorks with respect to each axis. Flexural rigidity was calculated using the second moments of area and elastic modulus values for bighorn sheep horn and cortical bone (Equation 1) (Carter and Hayes, 1977; Fuller and Donahue, 2021; Huang et al., 2019, 2017). Horn and bone were assigned elastic moduli of 1.8 GPA (Huang et al., 2017; Kitchener, 1988) and 20.5 GPa (Carter and Hayes, 1977; Fuller and Donahue, 2021), respectively. Flexural rigidity ratios, D_F/D_S, D_F/D_T, and D_T/D_S were determined as an indication to the relative directional resistance to bending.

$$D = (E_{Horn} * I_{Horn}) + (E_{Bone} * I_{Bone}) \quad (1)$$

In addition to the anatomically-relevant sagittal, frontal, and transverse plane analyses, the polar second moment of area and the maximum principal second moment of areas were computed. These geometrical properties were determined for each cross-section normal to the center line.

2.6 Finite Element Modeling

A representative 3D model of a solid horn and half sphere skull was created in Fusion 360 using a segmented and smoothed horn and skull derived from the geometry implemented by Drake et al. (2016). Briefly, the centerline and four of the horn cross-sections (10% cross-section, 30% cross-section, 60% cross-section, and 90% cross-section) were converted into an analytical surface, which was merged with a half sphere to produce a symmetric, simplified half-head model (Figure 4). Similar to our previously validated finite element model of bighorn sheep ramming in Drake et al. (Drake et al., 2016), we developed and employed a dynamic, symmetric impact model in Abaqus/Explicit (Dassault Systèmes). The horn, half sphere, and impact plate were all modeled as solid keratin ($E = 2$ GPa, $\nu = 0.3$, density of 1.3 g/cm^3) and the friction coefficient was defined as 0.1 between the impact surfaces (horn and impact plate) (Drake et al., 2016; Huang et al., 2017; Tombolato et al., 2010; Trim et al., 2011). An initial velocity of 5.7 m/s was applied to the half head structure (Drake et al., 2016). Symmetric boundary conditions about the y-z (sagittal) plane were applied to the horn and impact plate, with additionally restricted degrees of freedom of zero displacement in the y-direction (dorsal-ventral axis) and zero rotation about the x-axis (rotation in the sagittal plane). The baseline half head model was constructed of 59,394 second order, eight-node tetrahedral elements. This mesh density was determined from a mesh convergence study that showed a 1-3% difference in maximum translational acceleration, maximum von Mises stress, and maximum strain energy density when increasing the element number to 98,882 elements. Full mesh convergence results are provided in the appendix (Table A1).

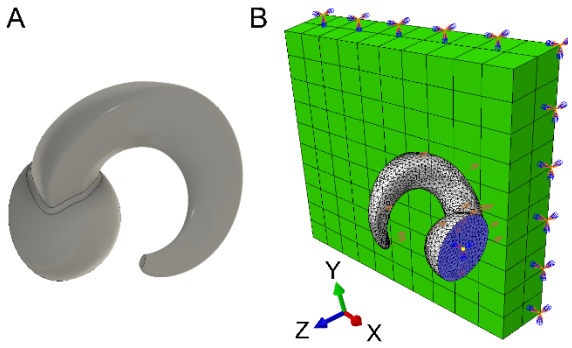

Figure 4. A) Representative, simplified half head model as an analytical surface. B) Baseline finite element impact model mesh and boundary conditions. The yellow dot in B shows the location of the sphere center point, which represents the brain center.

In addition to the baseline model, two additional horn shape geometries were developed – one with a circular cross-section and one with the bighorn sheep horn cross-section rotated 90º about the centerline from its natural orientation (Figure 5). To maintain consistency in impact timing, the first third of the horn geometry was kept consistent. The volume was consistent across all three models by defining the altered cross-sections as the same area as the baseline cross-sections. Model outputs included the following specific values for the center point of the half sphere (brain cavity center): fifteen milisecond head injury criterion (HIC_{15}, Equation 2, where t_2 and t_1 are time points 0.015 seconds apart that maximize the HIC value for each

simulation, and a(t) is acceleration in multiples of gravity), reaction force, and reaction torque. The maximum center point reaction force and reaction torque integrated over 0.015 second intervals were also determined for comparison in contrast to HIC_{15} values. In addition, the top 1% of nodal velocity values and element von Mises stresses were also computed, along with the fraction of model kinetic energy to total energy. The top 1% of velocity and stress values were chosen since single element or single nodal values may not be representative of comprehensive simulation results.

$$HIC = \max\left[\frac{1}{t_2 - t_1}\int_{t_1}^{t_2} a(t)dt\right]^{2.5}(t_2 - t_1) \quad (2)$$

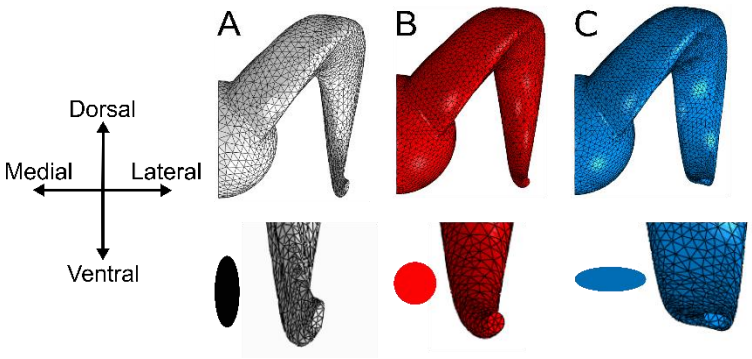

Figure 5. Symmetric finite element model geometries. Below each model is a zoomed view of the horn tip and approximated horn tip cross-sectional shape shown at left. All models have the same geometry for the first ~1/3rd of horn length to ensure initial impact is consistent across models. A) Baseline model of native bighorn sheep horn shape, with horn tip elongated in dorsal-ventral direction. B) Circular model with the distal two-thirds of the model having circular cross-sections. C) Rotated model with the distal two-thirds of the model having the native horn geometry rotated by 90° about the horn centerline.

2.7 Statistics

We hypothesized that the ratio of frontal to sagittal flexural rigidity would be significantly greater than one at the tip of the horn (last 10%) based on a medial-lateral bending motion observed during ramming, and that the remaining ratios would not be statistically different from one. To test this hypothesis, we conducted a one-sample t-test with a hypothesized value of one and α=0.05.

3. Results

The maximum principal and polar second moment of areas of each cross section showed similar trends across the keratin-rich horn and boney horncore (Table 1). Specifically, the horn max principal and polar second moment of areas initially increased to a maximum value at 30% of horn length, then decreased to a minimum at 90% of horn length. For horncore bone, these values continuously decreased from a maximum at 10% of horn length through 50% of horn

length, where the horncore ends (Table 1). Values were most similar between horn and bone at the base (10%, Table 1). Horn centerline length and lateral excursion were 521 ± 74 mm and 164 ± 29 mm, respectively (mean ± standard deviation).

Table 1. Max principal second and polar second moment of areas as a function of horn length. Data are presented as mean with standard deviation.

Horn Length	Max Principal [$m^4 *10^{-5}$]		Polar [$m^4 *10^{-5}$]	
	Horn	Bone	Horn	Bone
10%	0.487 ± 0.051	0.351 ± 0.16	0.442 ± 0.14	0.339 ± 0.16
20%	0.699 ± 0.078	0.214 ± 0.070	0.759 ± 0.081	0.187 ± 0.066
30%	0.712 ± 0.097	0.106 ± 0.044	0.874 ± 0.21	0.090 ± 0.033
40%	0.677 ± 0.17	0.0337 ± 0.017	0.832 ± 0.31	0.032 ± 0.012
50%	0.597 ± 0.20	0.00805 ± 0.0043	0.513 ± 0.29	0.00852 ± 0.0044
60%	0.381 ± 0.16	-	0.287 ± 0.094	-
70%	0.226 ± 0.12	-	0.156 ± 0.068	-
80%	0.110 ± 0.063	-	0.0914 ± 0.055	-
90%	0.0414 ± 0.037	-	0.0415 ± 0.040	-

For the anatomical second moment of area calculations, horn structures generally exhibited similar values for the bone and horn components at 10% of their length (base) (Table 1, Figure 6A-C). Bone second moment of area decreased with horn length until the horncore ends, at approximately 40-50% of total horn length (Figure 6C). These decreases were largely nonlinear due to the second-order relationship between the radius and second moment of area of a cross-section. Horn second moment of area increased briefly with length before decreasing greatly towards the tip, and was maximum at 30% for I_S and I_F and 20% for I_T (Figure 6). The flexural rigidity of the whole composite structure decreased from 10% to 90% of its length about all three axes (Figure 6D-F). The bending mechanics (flexural rigidity) are largely dominated by bone near the base (10% of length) and completely dominated by horn near the horn tip (90% of length) (Figure 6D-F). The point at which the flexural rigidity transitions from having a greater contribution of bone to a greater contribution of horn is between 30-40%, and by 60% all horns were 100% horn (Figure 6D-F).

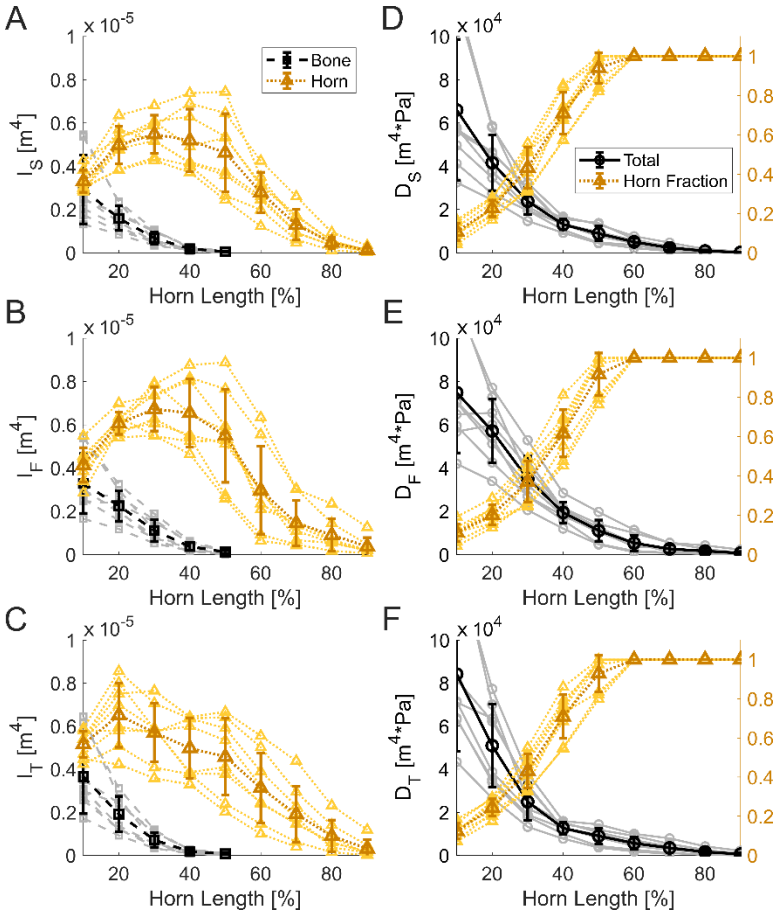

Figure 6. Second moments of area (I) (A-C) and flexural rigidity (D) (D-F) along all horns from proximal base (10%) toward distal end (90%). Subscripts I/D_S, I/D_F, and I/D_T denote second moments of area and flexural rigidity ratios for bending about the sagittal, frontal, and transverse axes, respectively, as shown in Figure 3. Second moment of area graphs provide bone (dashed black curves with square markers) and horn (dotted brown curves with triangle markers) second moment of area values separately. Flexural rigidity graphs provide combined values from both bone and horn (solid black curves with circle markers) and the fraction of the total flexural rigidity associated with the horn (dotted brown curves with triangle markers). Raw data are presented in the background with mean and standard deviation more prominent in the foreground.

The greatest flexural rigidity ratio at the horn tip – where the greatest amount of deformation occurs (Drake et al., 2016) – was found to be D_F/D_S, which would promote medial-lateral bending over dorsal-ventral bending (Figure 7A). Bending preference is approximately one through most of the horn length (Figure 7). There were differences ($p<0.05$) between the ratios and an assumed ratio of one (no bending preference) from 10-50% and 80-90% for D_F/D_S, 10-20% and 70-80% for D_T/D_S, and 20-50% and 80% for D_F/D_T (Figure 7). The greatest flexural rigidity ratio was D_F/D_S at 90%, with a value of 2.85 ± 1.2 ($p = 0.006$).

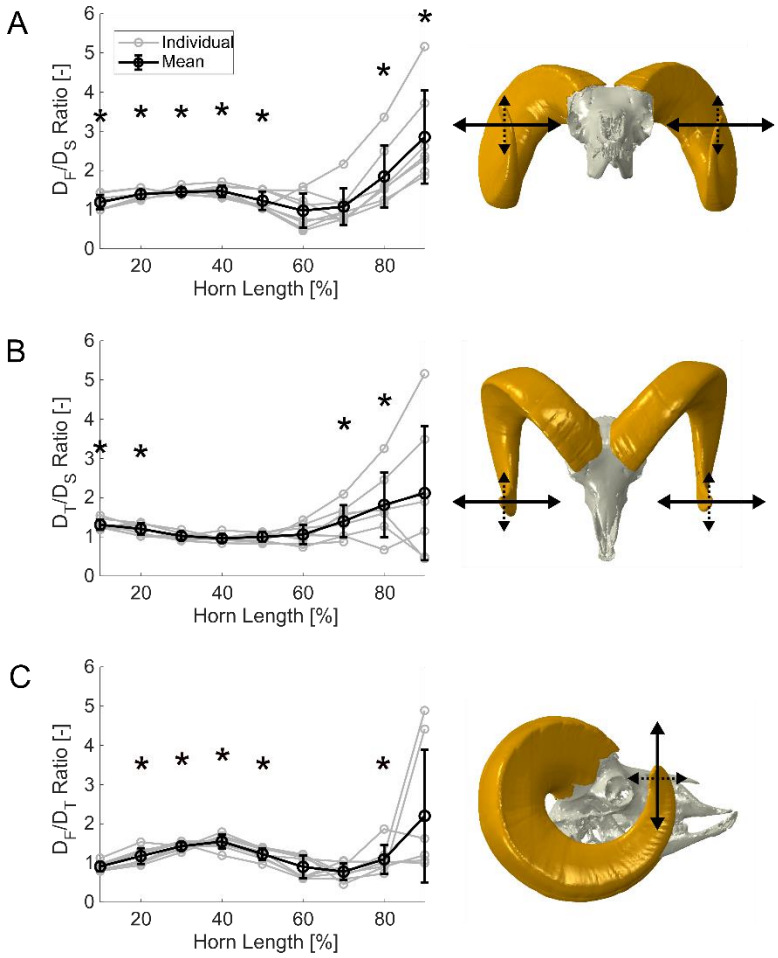

Figure 7. Flexural rigidity ratios (D_i/D_j) along all horns from the proximal (10%) to distal (90%) ends. A ratio greater than one indicates a bending preference in the direction of the solid arrows with respect to the dashed arrows. A) For D_F/D_S, a value above one indicates a medial-lateral bending is preferred over dorsal-ventral bending. B) For D_T/D_S, a value above one indicates medial-lateral bending is preferred over cranial-caudal bending. C) For D_F/D_T, a value above one indicates a cranial-caudal bending preference over a dorsal-ventral bending preference. Each * denotes a value different ($p<0.05$) from 1.

Finite element simulation results showed that the baseline model, in comparison to the circular or rotated models (Figure 5), exhibited the lowest brain center translational accelerations at impact (Figure 8). Specifically, the circular and rotated models exhibited 5% and 9% greater peak acceleration, respectively. The center HIC_{15} values were also the lowest in the baseline model (Table 2). Specifically, the circular and rotated models exhibited a 125% and 48% greater HIC_{15}, respectively. Brain center point reaction force and reaction moment area under the curves were also lowest in the baseline model, by 4-14% (Table 2). Maximum velocity was greatest in the baseline model (circular – 7% lower, rotated – 11% lower, Table 2). Maximum von Mises stress was greatest in the rotated model and lowest in the circular model, though these were within 4% of the baseline value (Table 2). Finally, the baseline model exhibited the greatest percentage of total model energy as kinetic energy at 91.4% (circular – 89.6%, rotated – 88.5%,

Table 2).

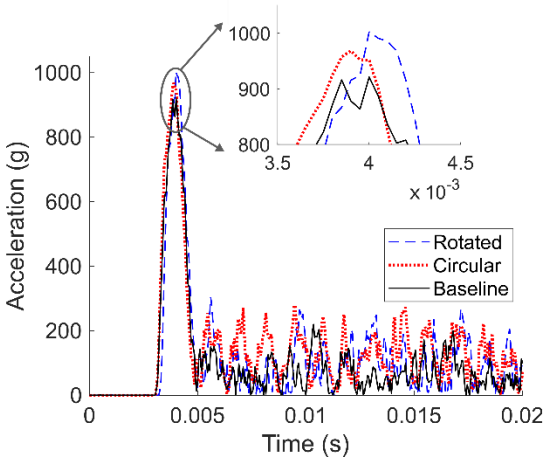

Figure 8. Brain center point translational accelerations for the baseline (solid black), circular (dotted red), and rotated (dashed blue) models. Impact occurs at approximately 4 ms.

Table 2. Finite element model outputs across three different horn shapes. Here HIC_{15} denotes the head injury criterion over 15 ms for each model center point, RF AUC denotes the reaction force area under the curve for each model brain center point, RM AUC denotes the reaction moment area under the curve for each model brain center point, Velocity denotes the maximum value of nodal velocities across the top 1% of all model nodes, Mises Stress denotes the maximum value of element von Mises stress across the top 1% of all elements, and KE fraction denotes the average percentage of model total energy that is kinetic energy.

Model	HIC_{15} [s-$g^{2.5}$]	RF AUC [N-s]	RM AUC [N-m-s]	Velocity [m/s]	Mises Stress [MPa]	KE Fraction [%]
Baseline	2780	160	25.3	28.9	27.5	91.4
Circular	6260	167	27.7	26.8	26.3	89.6
Rotated	4120	178	28.8	25.8	28.0	88.5

Each model exhibited distinctly different horn tip displacements and velocities following impact. The baseline model exhibited distinct medial-lateral oscillations, while the rotated model exhibited a mix of dorsal-ventral and cranial-caudal oscillations (Figure 9). The circular model exhibited a less structured deformation, with tip oscillations that varied between orientations following impact. The baseline modelling results corroborate the flexural rigidity results (Figure 7), which show a distinct medial-lateral bending preference. Specifically, it is clear that for the baseline model the horns oscillate in the medial-lateral direction due to this bending preference at the horn tip, which is not observed in the circular or rotated models. This medial-lateral horn tip oscillation thus reduces the reaction forces and moments at the brain cavity center, translational accelerations at the brain cavity center (Figure 8), and the head injury criterion (HIC_{15}; Table 2). Additionally, the medial-lateral horn tip oscillation is associated with

a greater horn tip velocity than the other models, and thus a greater fraction of total model energy is kinetic energy (due to greater velocities).

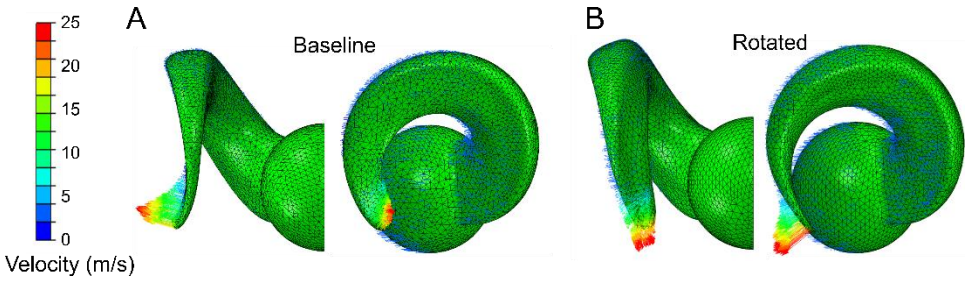

Figure 9. Representative horn tip velocity vectors following impact. A) Baseline model, with predominantly medial-lateral horn tip motion. B) Rotated model, with predominantly cranial-caudal horn tip motions. The circular model did not exhibit a clear preferred horn tip motion.

4. Discussion

The goals of this work were to 1) quantify male bighorn sheep horn shape across multiple individuals, and 2) determine the effect of various tapered spiral geometries for impact mitigation purposes. We used a custom shape characterization technique that compared inherent horn shape characteristics using anatomically relevant planes to better understand similarities in horn shapes and bending properties across different individuals. We then developed and implemented finite element analysis to study the effect of variations in tapered spiral horn shapes on impact mechanics with a simplified, symmetric half-head model. Our results showed that male bighorn sheep horns exhibit a clear medial-lateral bending preference that is consistent across individuals, and that altering the cross-sectional shape of the horn to reduce this medial-lateral preference has negative effects on impact mitigation.

This study is not without limitations and assumptions. We chose to compare flexural rigidity ratios, not flexural rigidity values, to normalize for differences in animal size, which increased the variance of the data. The finite element simulations performed in this work present a simplified impact analysis for the purposes of comparing the effects of different tapered spiral shapes on impact mitigation, and not a complete bighorn sheep skull and horns or ramming event. Thus, we did not attempt to fully characterize the intricate anatomical geometry, structure, material properties, and boundary conditions of such a phenomenon. For example, we did not include a point mass and neck spring as previously employed (Drake et al., 2016), as the specifics of these assumptions may confound the effects of various horn shapes. Additionally, we modeled impact as idealized in the cranial-caudal direction, and other impact directions could be an area of future study. We also fixed rotational boundary conditions at the center point due model simplifications, which prevented analyzing rotational accelerations in addition to translational accelerations. Our sample size of four individuals is somewhat small, although the major findings of this work are unlikely to be affected by this limitation.

One noteworthy assumption is of a homogeneous, nonporous, linear elastic material (keratin, E = 2 Gpa, ν = 0.3, density of 1.3 g/cm^3) for the half sphere and horn in our finite element model, in keeping with our prior validated finite element model of bighorn sheep ramming (Drake et al., 2016). Our constitutive model and parameters were chosen based on the work of Tombolato et al., 2010, who used an experimental three-point bending approach to determine that dry bighorn sheep keratin is highly linear with an elastic modulus from 1.7-2.2 GPa, which is supported by other studies (Huang et al., 2019, 2017; Trim et al., 2011). Furthermore, Huang et al., 2017 found that bighorn sheep keratin elastic modulus does not exhibit a high degree of strain rate variability, only ranging from ~1-3.5 Gpa across six orders of magnitude of strain rate variability. We assumed zero porosity for keratin in our impact finite element model due to the densely packed structure of keratin (observed porosity of 6-7%) (Trim et al., 2011) and in keeping with prior finite element modeling of keratin horn and hoof (Drake et al., 2016; Jansová et al., 2015; Johnson et al., 2021; Maity and Tekalur, 2011). Recently published finite element modeling of bighorn sheep ramming also used a nearly identical constitutive model (homogeneous, zero porosity, linear elastic, E = 2.2 GPa, ν = 0.3, density 1.2 g/cm^3) (Johnson et al., 2021).

This study focused on shape characterization of bighorn sheep horn cross-sectional geometry for the purpose of understanding how horn shape contributes to post-impact horn deformations and parameters related to traumatic brain injury (head injury criterion – HIC). We aimed to determine how bighorn sheep horn shape may be similar across individuals, and thus how these structures might be adapted to mitigate brain cavity accelerations after ramming in the wild. We hypothesized that horn geometry would transition from having little bending preference at the base to a medial-lateral bending preference at the horn tip. Broadly, our findings support this hypothesis (Figure 7), with greater numerical analysis provided below. Previous modeling work has shown that following impact, bighorn sheep horns exhibit medial-lateral horn tip oscillations (Drake et al., 2016). Using a combined shape characterization and finite element modeling approach, we have shown that this medial-lateral bending preference (Figure 7) causes medial-lateral horn tip oscillations in comparison to other horn tip geometries (Figure 9). Medial-lateral horn tip oscillations are associated with reduced impact accelerations and HIC_{15} values, thus we suggest these oscillations may play an important role in preventing or limiting brain injury in bighorn sheep. Designing safety equipment such as helmets with bioinspired structures that mimic the elastic energy dissipating mechanisms of bighorn sheep horns may improve impact performance and mitigate brain injury in humans.

Flexural rigidity is a measurement of a structure's resistance to bending and incorporates material properties (the elastic modulus) and geometrical properties (the second moment of area) (Equation 1). Since the bighorn sheep horn structure is a composite of bone and horn (keratin), we used a custom shape characterization approach to determine the second moment of area properties of bone and horn cross-sections separately along the length of each structure (Figures 2-3). Next, we applied composite beam theory and the parallel axis theorem to determine the combined flexural rigidity of each cross-section relative to the three anatomical planes (Figure 1

and 3). The maximum principal second moment of area and polar second moment of area were also quantified to roughly characterize cross sectional properties independent of anatomical planes. Previous modeling work has shown that removal of the velar bone structure in the horncore can have dramatic effects on brain cavity accelerations and horn strains during and after impact (Drake et al., 2016). Results in this study show that the boney horncore runs approximately 50% of the total horn length and has the largest second moment of area values proximally (~$0.35*10^{-5}$ m^4), where the horncore dominates the flexural rigidity of the structure (Table 1; Figure 6). These findings were consistent across the four individuals observed in this study, which supports the previous suggestion that horncore bone plays a vital role in impact mechanics of bighorn sheep horns. Previous work also demonstrated that removal of the distal half of the horn increases brain cavity accelerations post impact. Since the flexural rigidity of the distal half of the horn structure is dictated by the keratin-rich horn (Table 1, where bone second moment of area values above 50% are zero and Figure 6, where flexural rigidity is keratin-only after 50%), it is clear that both the horn and horncore play pivotal roles in mitigating the effects of impact, though further dissection of contributions from bone and keratin are outside the scope of this work.

The flexural rigidity ratio between the frontal and sagittal axes, which is a measurement of the preference of the horn to bend in the medial-lateral versus dorsal-ventral directions, was greatest at the horn tip (2.85) and had a limited preference at the base (1.19) (Figure 7). Due to the large, boney cross-section at 10% total length (Figure 6), there is relatively little deformation at the base of the horn relative to the horn tip from impacts (Figure 9) (Drake et al., 2016). Our finite element modeling results show that this medial-lateral bending preference facilitates medial-lateral horn tip oscillations of approximately 25 m/s observed for the baseline horn geometry (Figure 9). Conversely, there is a mix of dorsal-ventral and cranial-caudal oscillations seen in the rotated model geometry (Figure 9) while randomly oriented oscillations are displayed in the circular model. In addition to medial-lateral oscillations, greater peak velocities (28.9 m/s versus <27 m/s) and kinetic energy fraction (91.4% versus >90%) were observed for the baseline model (Table 2). Crucially, the circular and rotated models produced HIC_{15} values 125% and 48% greater than the baseline model, respectively. These rather large differences in HIC_{15} values highlight how subtle changes to the geometry of energy dissipating structures can greatly affect payload mechanics (in this case model center point or brain cavity approximation). Furthermore, the baseline model exhibited lower reaction forces (area under the curve of 160 N-s for the whole simulation versus 167+ N-s) and reaction moments (25.3 N-m-s versus 27.7+ N-m-s) at the center point (Table 2), suggesting that the differences in center point acceleration (Figure 8) and HIC_{15} (Table 2) values may be greater in a less constrained model. These observed model differences are clearly due to variations in horn tip geometry, as the total horn volume for all three models were nearly identical and each model exhibited the same boundary conditions, material properties, horn geometry at the point of impact, and horn centerline.

High velocity horn tip oscillations could be beneficial for mitigating the effects of impact as they dissipate impact energy, which in turn reduces brain cavity accelerations, head injury

criterion (HIC_{15}), and the likelihood of brain injury. However, this is only the case if such oscillations occur in specific directions, leveraging symmetry or other boundary conditions and do not further contribute to brain cavity accelerations. This phenomenon is shown in the medial-lateral oscillations and lower HIC_{15} in the baseline model compared to the dorsal-ventral and cranial-caudal oscillations associated with higher HIC_{15} in the rotated model (Table 2; Figure 9). The geometry of the baseline model thus has superior impact mitigating properties through two main mechanisms – 1) medial-lateral oscillations that leverage the symmetry of the head and paired horn structure, and 2) increased kinetic energy, and thus greater energy dissipation, through greater horn tip velocities.

Finally, the maximum von Mises stress of approximately 26-28 MPa is similar across models (Table 2) and falls within the measured range of yield stress reported for bighorn sheep horn across dry/wet and tensile/compressive conditions (3.7-72.1 MPa) (Trim et al., 2011). While our simplified model does not aim to predict whether or not horn failure occurs from ramming, the observation of similar maximum von Mises stress suggests that material failure is equally likely across all model geometries. Thus, increased impact mitigation does not necessarily come at the cost of greater material stress in the horn and horncore. This finding is crucial for leveraging bighorn sheep horn shapes for bioinspired devices and applications, as the horn tip oscillations dissipate impact energy through elastic deformations, in comparison to many impact systems that utilize material damage to dissipate energy (such as a car bumper). Our prior modeling work (Drake et al., 2016) also detailed stress distributions in bighorn sheep skull and horns throughout impact, which was not a focus of this work.

While studies of bighorn sheep impact biomechanics are limited, comparing our results to previously published works further supports our findings. Tapered spirals have been previously shown to exhibit preferable structural properties for energy dissipation in comparison to simpler shapes such as a spiral or tapered cylinder (Johnson et al., 2014). Our work suggests that designing directionally tapered spirals would further improve energy dissipation, and future work to explore other horn shape variations would greatly benefit the field. Our peak acceleration value for the baseline model (921 gs, Figure 8) is comparable to recent modeling work investigating the effect of dry and wet keratin on sheep impact mechanics of 607 gs in a fully developed model (Johnson et al., 2021). It is not surprising that our model predicted higher accelerations, as we employed a simplified, keratin-only structure. It should be noted that accelerations of ~900 gs are considerably higher than the threshold for impacts that could cause injury to a human brain (~100 gs) (King et al., 2003) or would be experienced during extreme events such as a professional American football extreme impact (~250 gs maximum) (Greenwald et al., 2008). When comparing the HIC_{15} values observed here (>2,700 s-$g^{2.5}$, Table 2) to American football impacts (maximum ~800 s-$g^{2.5}$), again the values exceed those that would be expected. However, the purpose of this study was not to reproduce specific impact conditions, but to compare different horn shapes.

The findings of our work can be leveraged to design bioinspired impact mitigating structures across broad applications. For example, paired oscillating systems that absorb impact in one direction and direct it into synchronous oscillations in a perpendicular direction may be effective strategy for dissipating energy in impact conditions (helmets, car bumpers, etc.). Another advantage to the energy dissipation approach highlighted in this study is the elastic deformation of bighorn sheep horns during impact and the reuse of horns for repeated impacts. Elastic deformations suggest that such structures could be used to repeatedly mitigate the effects of impacts in comparison to systems such as bicycle helmets and car bumpers, which are designed to accumulate damage under extreme impacts.

5. Conclusion

Concussions are a major problem according to the CDC, particularly for athletes (American football, soccer, rugby, etc.) and military personnel (DePadilla, 2018; "Report to Congress on Traumatic Brain Injury in the United States," 2019). Brain cavity accelerations have been linked to brain injuries such as a concussion or chronic traumatic encephalopathy and the head injury criterion (HIC_{15}) is one frequently used measurement of brain cavity accelerations during impact (Hutchinson et al., 1998; Meaney and Smith, 2011). The shape of bighorn sheep horns promotes bending in medial-lateral directions, which then result in medial-lateral horn tip oscillations following impact. These high-velocity directional oscillations dissipate impact energy, thus mitigating brain cavity accelerations and lowering HIC_{15}. This effect can be shown by comparing impact mechanics of native bighorn sheep horns to impact mechanics of different horn shapes that do not exhibit a medial-lateral bending preference. These findings can be used for bioinspired design of horn-like structures to mitigate the effects of impacts. Future studies to explore further variations in horn geometry, size, and location during impact to assess the optimal horn-like geometric parameters would be a considerable benefit to the field.

6. Acknowledgements

Authors would like to acknowledge Sai Pranav Rallabhandi for efforts in the development of a procedure to characterize horn shape during the early stages of this work.

7. Appendix

Table A1. Full baseline mesh convergence results, comparing element number, model run time, maximum acceleration of the brain center point, maximum model Mises stress, and maximum strain energy fraction. The bolded model with 59,394 elements was selected for analysis.

Number of	Run Time	Max Acceleration	Next Model	Max Mises	Next Model	Max Strain	Next Model Difference

Elements	[hrs]	[g]	Difference [%]	Stress [MPa]	Difference [%]	Energy Fraction [-]	[%]
5568	0.75	8598	-6.0%	42.6	-13%	0.666	-0.7%
9760	2.4	9146	4.2%	48.8	8.8%	0.671	1.0%
25874	5.4	8776	-2.9%	44.9	-6.5%	0.664	0.8%
59394	**5.7**	**9036**	**0.8%**	**48.0**	**3.2%**	**0.659**	**-0.1%**
98882	16.4	8966	-1.1%	46.5	-2.0%	0.659	0.1%
140082	19.1	9063	-	47.5	-	0.659	-

8. References

Ackermans, N.L., Varghese, M., Williams, T.M., Grimaldi, N., Selmanovic, E., Alipour, A., Balchandani, P., Reidenberg, J.S., Hof, P.R., 2022. Evidence of traumatic brain injury in headbutting bovids. Acta Neuropathol. (Berl.) 144, 5–26. https://doi.org/10.1007/s00401-022-02427-2

Aguirre, T.G., Fuller, L., Ingrole, A., Seek, T.W., Wheatley, B.B., Steineman, B.D., Donahue, T.L.H., Donahue, S.W., 2020. Bioinspired material architectures from bighorn sheep horncore velar bone for impact loading applications. Sci. Rep. 10, 18916. https://doi.org/10.1038/s41598-020-76021-5

Broglio, S.P., Schnebel, B., Sosnoff, J.J., Shin, S., Fend, X., He, X., Zimmerman, J., 2010. Biomechanical properties of concussions in high school football. Med. Sci. Sports Exerc. 42, 2064–2071. https://doi.org/10.1249/MSS.0b013e3181dd9156

Broglio, S.P., Sosnoff, J.J., Shin, S., He, X., Alcaraz, C., Zimmerman, J., 2009. Head impacts during high school football: a biomechanical assessment. J. Athl. Train. 44, 342–9. https://doi.org/10.4085/1062-6050-44.4.342

Carter, D.R., Hayes, W.C., 1977. The compressive behavior of bone as a two-phase porous structure. J. Bone Joint Surg. Am. 59, 954–962.

Cignoni, P., Callieri, M., Corsini, M., Dellepiane, M., Ganovelli, F., Ranzuglia, G., 2008. MeshLab: an Open-Source Mesh Processing Tool. The Eurographics Association. https://doi.org/10.2312/LocalChapterEvents/ItalChap/ItalianChapConf2008/129-136

Daneshvar, D.H., Goldstein, L.E., Kiernan, P.T., Stein, T.D., McKee, A.C., 2015. Post-traumatic neurodegeneration and chronic traumatic encephalopathy. Mol. Cell. Neurosci. 66, 81–90. https://doi.org/10.1016/j.mcn.2015.03.007

DePadilla, L., 2018. Self-Reported Concussions from Playing a Sport or Being Physically Active Among High School Students — United States, 2017. MMWR Morb. Mortal. Wkly. Rep. 67. https://doi.org/10.15585/mmwr.mm6724a3

Drake, A., Haut Donahue, T.L.T.L., Stansloski, M., Fox, K., Wheatley, B.B.B., Donahue, S.W.S.W., 2016. Horn and horn core trabecular bone of bighorn sheep rams absorbs impact energy and reduces brain cavity accelerations during high impact ramming of the skull. Acta Biomater. 44, 41–50. https://doi.org/10.1016/j.actbio.2016.08.019

Farah, G., Siwek, D., Cummings, P., 2018. Tau accumulations in the brains of woodpeckers. PLOS ONE 13, e0191526. https://doi.org/10.1371/journal.pone.0191526
Finkbeiner, N.W.B., Max, J.E., Longman, S., Debert, C., 2016. Knowing What We Don't Know: Long-Term Psychiatric Outcomes following Adult Concussion in Sports. Can. J. Psychiatry Rev. Can. Psychiatr. 61, 270–276. https://doi.org/10.1177/0706743716644953
Fuller, L.H., Donahue, S.W., 2021. Material properties of bighorn sheep (Ovis canadensis) horncore bone with implications for energy absorption during impacts. J. Mech. Behav. Biomed. Mater. 114, 104224. https://doi.org/10.1016/j.jmbbm.2020.104224
Geist, V., 1974. Mountain Sheep: A Study in Behavior and Evolution. University of Chicago Press.
Geist, V., 1966. Validity of Horn Segment Counts in Aging Bighorn Sheep. https://doi.org/10.2307/3798763
Greenwald, R.M., Gwin, J.T., Chu, J.J., Crisco, J.J., 2008. Head impact severity measures for evaluating mild traumatic brain injury risk exposure. Neurosurgery 62, 789–98; discussion 798. https://doi.org/10.1227/01.neu.0000318162.67472.ad
Guskiewicz, K.M., Mihalik, J.P., Shankar, V., Marshall, S.W., Crowell, D.H., Oliaro, S.M., Ciocca, M.F., Hooker, D.N., 2007. Measurement of head impacts in collegiate football players: relationship between head impact biomechanics and acute clinical outcome after concussion. Neurosurgery 61, 1244–52; discussion 1252-3. https://doi.org/10.1227/01.neu.0000306103.68635.1a
Ha, N.S., Lu, G., 2020. A review of recent research on bio-inspired structures and materials for energy absorption applications. Compos. Part B Eng. 181, 107496. https://doi.org/10.1016/j.compositesb.2019.107496
Huang, W., Zaheri, A., Jung, J.-Y., Espinosa, H.D., Mckittrick, J., 2017. Hierarchical structure and compressive deformation mechanisms of bighorn sheep (Ovis canadensis) horn. Acta Biomater. 64, 1–14. https://doi.org/10.1016/j.actbio.2017.09.043
Huang, W., Zaheri, A., Yang, W., Kisailus, D., Ritchie, R.O., Espinosa, H., McKittrick, J., 2019. How Water Can Affect Keratin: Hydration-Driven Recovery of Bighorn Sheep (Ovis Canadensis) Horns. Adv. Funct. Mater. 29, 1901077. https://doi.org/10.1002/adfm.201901077
Hutchinson, J., Kaiser, M.J., Lankarani, H.M., 1998. The Head Injury Criterion (HIC) functional. Appl. Math. Comput. 96, 1–16. https://doi.org/10.1016/S0096-3003(97)10106-0
Islam, M.K., Hazell, P.J., Escobedo, J.P., Wang, H., 2021. Biomimetic armour design strategies for additive manufacturing: A review. Mater. Des. 205, 109730. https://doi.org/10.1016/j.matdes.2021.109730
Jansová, M., Ondoková, L., Vychytil, J., Kochová, P., Witter, K., Tonar, Z., 2015. A Finite Element Model of an Equine Hoof. J. Equine Vet. Sci. 35, 60–69. https://doi.org/10.1016/j.jevs.2014.11.008
Johnson, K.L., Trim, M.W., Horstemeyer, M.F., Lee, N., Williams, L.N., Liao, J., Rhee, H., Prabhu, R., 2014. Geometric Effects on Stress Wave Propagation. J. Biomech. Eng. 136, 021023–021023. https://doi.org/10.1115/1.4026320
Johnson, K.L., Trim, M.W., Mao, Y., Rhee, H., Williams, L.N., Liao, J., Griggs, J., Horstemeyer, M.F., Duan, Y., 2021. Finite element analysis of a ram brain during impact under wet and dry horn conditions. J. Mech. Behav. Biomed. Mater. 104400. https://doi.org/10.1016/j.jmbbm.2021.104400

King, A., Yang, K., Zhang, L., Hardy, W., 2003. Is Head Injury Caused by Linear or Angular Acceleration? Presented at the IRCOBI.

Kitchener, A., 1988. An analysis of the forces of fighting of the blackbuck (Antilope cervicapra) and the bighorn sheep (Ovis canadensis) and the mechanical design of the horn of bovids. J. Zool. 214, 1–20. https://doi.org/10.1111/j.1469-7998.1988.tb04983.x

Lee, N., Horstemeyer, M.F., Prabhu, R., Liao, J., Rhee, H., Hammi, Y., Moser, R.D., Williams, L.N., 2016. The geometric effects of a woodpecker's hyoid apparatus for stress wave mitigation. Bioinspir. Biomim. 11, 066004. https://doi.org/10.1088/1748-3190/11/6/066004

Maity, P., Tekalur, S.A., 2011. Finite element analysis of ramming in Ovis canadensis. J. Biomech. Eng. 133, 021009–021009. https://doi.org/10.1115/1.4003321

Meaney, D.F., Smith, D.H., 2011. Biomechanics of Concussion. Clin. Sports Med. 30, 19–vii. https://doi.org/10.1016/j.csm.2010.08.009

Mountain Sheep of North America [WWW Document], 2017. . UAPress. URL https://uapress.arizona.edu/book/mountain-sheep-of-north-america (accessed 8.6.21).

Naleway, S.E., Porter, M.M., McKittrick, J., Meyers, M.A., 2015. Structural Design Elements in Biological Materials: Application to Bioinspiration. Adv. Mater. 27, 5455–5476. https://doi.org/10.1002/adma.201502403

Panagiotopoulou, O., Spyridis, P., Abraha, H.M., Carrier, D.R., Pataky, T.C., 2016. Architecture of the sperm whale forehead facilitates ramming combat. PeerJ 4, e1895. https://doi.org/10.7717/peerj.1895

Pellman, E.J., Viano, D.C., Tucker, A.M., Casson, I.R., Waeckerle, J.F., 2003. Concussion in professional football: reconstruction of game impacts and injuries. Neurosurgery 53, 799–812; discussion 812-814. https://doi.org/10.1093/neurosurgery/53.3.799

Report to Congress on Traumatic Brain Injury in the United States: Understanding the Public Health Problem among Current and Former Military Personnel | Concussion | Traumatic Brain Injury | CDC Injury Center [WWW Document], 2019. URL https://www.cdc.gov/traumaticbraininjury/pubs/congress_military.html (accessed 8.6.21).

Snively, E., Theodor, J.M., 2011. Common Functional Correlates of Head-Strike Behavior in the Pachycephalosaur Stegoceras validum (Ornithischia, Dinosauria) and Combative Artiodactyls. PLOS ONE 6, e21422. https://doi.org/10.1371/journal.pone.0021422

Tombolato, L., Novitskaya, E.E., Chen, P.-Y., Sheppard, F.A., McKittrick, J., 2010. Microstructure, elastic properties and deformation mechanisms of horn keratin. Acta Biomater. 6, 319–30. https://doi.org/10.1016/j.actbio.2009.06.033

Trim, M.W., Horstemeyer, M.F., Rhee, H., El Kadiri, H., Williams, L.N., Liao, J., Walters, K.B., McKittrick, J., Park, S.-J., 2011. The effects of water and microstructure on the mechanical properties of bighorn sheep (Ovis canadensis) horn keratin. Acta Biomater. 7, 1228–40. https://doi.org/10.1016/j.actbio.2010.11.024

Wang, B., Yang, W., McKittrick, J., Meyers, M.A., 2016. Keratin: Structure, mechanical properties, occurrence in biological organisms, and efforts at bioinspiration. Prog. Mater. Sci. 76, 229–318. https://doi.org/10.1016/j.pmatsci.2015.06.001

Wang, L., Cheung, J.T.-M., Pu, F., Li, D., Zhang, M., Fan, Y., 2011. Why do woodpeckers resist head impact injury: a biomechanical investigation. PloS One 6, e26490–e26490. https://doi.org/10.1371/journal.pone.0026490

Zhou, J., Liu, S., Guo, Z., Xu, S., Song, J., Zou, M., 2021. Study on the energy absorption performance of bionic tube inspired by yak horn. Mech. Adv. Mater. Struct. 0, 1–13. https://doi.org/10.1080/15376494.2021.1995088